

Three-Dimensional Modeling of an Urban Park and Trees by Combined Airborne and Portable On-Ground Scanning LIDAR Remote Sensing

K. Omasa · F. Hosoi · T. M. Uenishi ·
Y. Shimizu · Y. Akiyama

Received: 26 July 2006 / Accepted: 2 June 2007 / Published online: 3 July 2007
© Springer Science + Business Media B.V. 2007

Abstract In this study, we confirmed the utility of airborne and portable on-ground scanning light detection and ranging (LIDARs) for three-dimensional visualization of an urban park and quantification of biophysical variables of trees in the park. The digital canopy height model (DCHM) and digital terrain model generated from airborne scanning LIDAR data provided precise images of the ground surface and individual tree canopies. The heights of 166 coniferous and broadleaf trees of 11 species in the park were estimated from the DCHM images with slight underestimation (mean error = -0.14 m, RMSE = 0.30 m). Portable on-ground scanning LIDAR provided images of individual trees with detailed features. Tree height and trunk diameter were estimated to be within 0.31 m and 1 cm, respectively, from the on-ground LIDAR images. We combined airborne and on-ground LIDAR images to overcome blind regions and created a complete three-dimensional model of three standing trees. The model allowed not only visual assessment from all viewpoints but also quantitative estimation of canopy volume, trunk volume, and canopy cross-sectional area.

Keywords Three-dimensional modeling · FP-mode DEM · DTM · Composite remote sensing · Scanning LIDAR · Tree measurement · Urban park · Visual assessment

1 Introduction

Urban parks provide social and psychological benefits to city dwellers and contribute to the amenity of urban environments. Time spent in parks can reduce stress, enhance contemplativeness, rejuvenate people, and provide peace and tranquillity [8, 16, 38]. The vegetation in parks can purify the air, reduce noise, and stabilize the microclimate [1, 17, 31]. Remote sensing from satellites and aircraft has been widely used to assess urban parks and functions of vegetation [10, 27]. While ordinary passive remote sensing provides useful two-dimensional information for assessments, three-dimensional data may improve understanding of the landscape and tree functions in urban parks [7, 13, 19, 26, 34]. Computer graphics is also capable for visual assessment of urban parks [6, 18]. By joining three-dimensional observation and computer graphics, it is possible to produce detailed three-dimensional visual models of landscapes and trees for visual assessment.

Light detection and ranging (LIDAR), which uses a laser scanner to measure the distance between the sensor and targets, is one of the most accurate tools for three-dimensional measurement. Airborne scanning LIDAR has been used to acquire three-dimensional information on landscapes and trees [20, 25, 29]. In particular, the use of helicopter-mounted scanning LIDAR with a small footprint and high pulse frequency allows the production of three-dimensional images with a resolution of several tens of centimeters and a precise grid [22, 28, 30]. The utility of

K. Omasa (✉) · F. Hosoi · T. M. Uenishi · Y. Shimizu
Graduate School of Agricultural and Life Sciences,
The University of Tokyo,
Yayoi 1-1-1,
Bunkyo-ku, Tokyo 113-8657, Japan
e-mail: aomasa@mail.ecc.u-tokyo.ac.jp

Y. Akiyama
Aero Asahi Co.,
Shinsayama 1-18-1 Sayama,
Saitama 350-1331, Japan

airborne scanning LIDAR has been also demonstrated in urban areas [9, 24]. Thus, it could be used for the three-dimensional reconstruction of an urban park. However, airborne LIDAR cannot capture some regions, such as the lower parts of trees, because the laser beams can be obscured by the upper canopy. These blind regions, i.e., the region that LIDAR cannot capture due to the obstruction of laser beam penetration by foliage or other tree tissues, might reduce the quality of the three-dimensional reconstruction and compromise the assessment of urban parks.

Meanwhile, portable on-ground scanning LIDAR has been used for three-dimensional reconstruction of objects [33, 35] and for tree measurements [11, 12, 21, 29, 32, 36]. On-ground scanning LIDAR could compensate for blind regions in airborne LIDAR data because its position on the ground allows capture of the lower regions of trees that airborne scanning LIDAR misses, but conversely, it may not capture some upper regions of trees. Thus, the combination of data from airborne and on-ground LIDARs would allow the creation of a complete three-dimensional model of trees without any blind regions.

In this study, we demonstrated the capabilities and limitations of high-resolution airborne scanning LIDAR and portable on-ground scanning LIDAR for three-dimensional visualization of an urban park and for quantification of biophysical variables of trees growing in the park. In addition, we produced a complete three-dimensional model of trees and computed more descriptive variables of the trees through the combination of airborne and on-ground LIDARs.

2 Materials and Methods

2.1 Study Site and Ground-Truth Data

We selected an urban park, the Shinjuku Gyoen National Garden in the center of Tokyo, as our study site (Fig. 1). About 250 species and 2,000 trees grow there. Tree height, trunk diameter, and canopy diameter were chosen as the representative variables to confirm LIDAR's ability to quantify tree variables in the park. Then, we trigonometrically measured the heights of 166 coniferous and broadleaf trees of 11 species on the ground in October 2001 with a range finder (Lasertape FG-21-HA, RIEGL, Austria) with an accuracy of ± 5 cm. We also measured the trunk diameter and canopy diameter of each tree by tape measure.

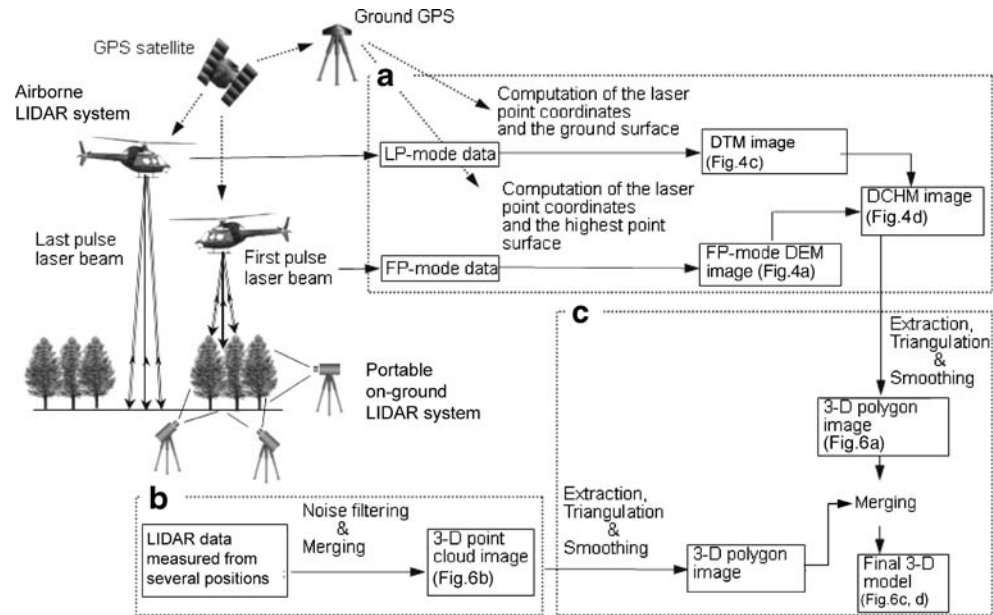
2.2 Airborne Scanning LIDAR Data

Figure 2 shows a schematic diagram of three-dimensional remote sensing by the combination of airborne and on-ground LIDAR data. High-repetition laser pulses were directed from a LIDAR mounted on a helicopter (ALTM 1225 special model, Optech and Aero Asahi, Japan [28, 30]) onto the canopy and ground surfaces at the study site. The distance to an object was calculated from the elapsed time between the emitted and returned pulses. This airborne LIDAR has two receiving modes: first-pulse mode (FP-mode) in which first returned pulses are detected and last-pulse mode (LP-mode) in which the last returned pulses are

Fig. 1 Aerial photograph of the Shinjuku Gyoen National Garden in Tokyo. 1 Three *Metasequoia glyptostroboides* (dawn redwoods; see Fig. 3). 2 *Liriodendron tulipifera* (yellow poplar). 3 *Prunus × yedoensis* (Yoshino cherry; see Fig. 5). The broken line shows the position of the French Formal Garden (see Fig. 4b)



Fig. 2 Schematic diagram of three-dimensional remote sensing by combined airborne and portable on-ground scanning LIDAR. **a** Generation of FP-mode DEM, DTM, and DCHM images from airborne scanning LIDAR data. **b** Generation of the three-dimensional point cloud image from the on-ground LIDAR data. **c** Merging of the airborne and on-ground LIDAR images



detected. Laser pulses illuminating the canopy surface were received as FP-mode data, which were used to generate an image of the woody outer canopy. Pulses that reached the ground surface were received as LP-mode data, which were used to generate a terrain image. The laser wavelength was 1,064 nm, and its repetition frequency was 25,000 Hz. The scanning frequency was set to 20 Hz. The scanning angle was 20.0°.

Using this system, we measured the study site (600×700 m) at a flight speed of 50 km/h and a flight height of 300 m in November 2001. The range accuracy was within 15 cm. The beam divergence was 1.0 mrad, and the footprint diameter on the ground was estimated to be about 30 cm. The footprint interval on the ground was 21.2 cm in the direction of the scan and 34.7 cm in the direction of flight. By comparing the diameter and interval of footprints on the ground, we could confirm that the laser pulses covered most of the woody canopy. The three-dimensional geographic position was determined from a helicopter-borne inertial measurement unit (IMU) and high-resolution global positioning system (GPS) receivers both in the helicopter and on the ground.

2.3 Portable On-ground Scanning LIDAR Data

Three *Metasequoia glyptostroboides* (dawn redwood) trees growing at the study site were measured from five ground measurement positions in October by portable on-ground scanning LIDAR (LPM-25HA range-finder, RIEGL), as shown in Fig. 3. *Liriodendron tulipifera* (yellow poplar) and *Prunus × yedoensis* (Yoshino cherry) were also measured from five and four ground positions, respectively. The positions were selected to surround the trees. The LIDAR could measure the distance to the surface of an

object between 2 and 60 m away, without the use of a reflector, using the elapsed time between the emitted and returned laser pulses. The laser beam diameter was 20 to 60 mm when the measuring distance was 20 to 60 m. The point at which the infrared (905 nm) laser for range measurement was aimed was determined from a visible red (~650 nm) laser pointer. A rotating mount run by a

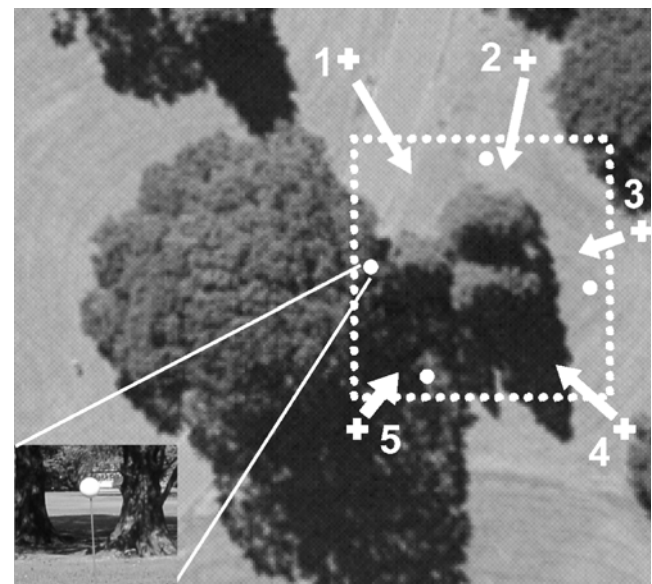


Fig. 3 Three *Metasequoia glyptostroboides* trees at the study site. The broken line shows the target area where the *M. glyptostroboides* grow. Five crosses and arrows indicate the measurement positions and scanning directions of the portable on-ground scanning LIDAR. Four white circles within the target area show the positions of tooling balls placed as references for merging the on-ground LIDAR data. The inset shows a close-up of the tooling ball. The huge tree on the left of the three trees is a *Liriodendron tulipifera*

built-in step motor with 0.009° accuracy that could pan and tilt the LIDAR head allowed angular movement of the instrument. The LIDAR had an accuracy of ± 8 mm in computing the range of each sample point.

2.4 Generation of Digital Models from Airborne Scanning LIDAR Data

Figure 2a shows the steps in generating the FP-mode digital elevation model (DEM), digital terrain model (DTM), and digital canopy height model (DCHM) of the study site. These models were produced with modified software made by TopScan, ERDAS IMAGINE (Leica Geosystems GIS & Mapping) and our own software from the airborne scanning LIDAR data. The point coordinates of both FP-mode and LP-mode data were determined from the GPS data coordinates recorded in the helicopter and on the ground. The DEM of the canopy surface was generated from FP-mode data. The DTM of the ground surface was generated by interpolating the extracted ground-level data from the LP-mode data. The DCHM was generated by subtracting the DTM from the FP-mode DEM [28, 30]. To remove spike noise, the image was pre-processed with a median filter with a mask size of 3×3 pixels.

The visual quality of the FP-mode DEM and DTM images was assessed by checking the shapes of constructions, trees, and the ground surface within the images. To confirm the airborne LIDAR's ability to quantify tree variables, we extracted the heights of 166 trees in 11 species by manually selecting treetops from the DCHM and comparing them with ground-truth data.

2.5 Merging of Portable On-Ground Scanning LIDAR Data

Figure 2b shows the steps in merging the on-ground LIDAR data. To remove spike noise, the data were pre-processed by a median filter with a mask size of 10×10 pixels, as determined according to the noise level. The data were then merged into a single coordinate system using the iterative closest point (ICP) algorithm [5]. This algorithm starts with an initial estimate of corresponding points between two LIDAR datasets measured from different positions. Based on the corresponding points, the data are co-registered through rigid-body transformation. The transform was then iteratively refined by alternately choosing corresponding points in the LIDAR data and finding the best translation and rotation matrices that minimize an error metric based on the distance between them. This procedure was used for all pairs of LIDAR data. Finally, LIDAR data from all positions were merged as a three-dimensional point cloud image, which is a set of points measured in three-dimensional space. A good initial estimate of the rigid-body transform is necessary to obtain an accurate point cloud

image. Therefore, we placed four tooling balls made from styrene foam around the standing trees for reference as shown in Fig. 3.

The visual quality of the images was assessed by checking the shapes of *L. tulipifera* and *P. × yedoensis* trees. For confirmation of the on-ground LIDAR's ability to quantify tree variables, we compared the LIDAR-derived heights and trunk diameters of three *M. glyptostroboides* trees with ground-truth data.

2.6 Merging Airborne and Portable On-Ground Scanning LIDAR Data

Figure 2c shows the steps in merging the airborne and on-ground LIDAR data. Three *M. glyptostroboides* trees were chosen for the merging because images of these trees obtained from both LIDARs included blind regions. We selected the portion of DCHM data that included the stand. To focus on the *Metasequoia* trees alone, we eliminated a huge *L. tulipifera* tree covering part of these trees (see Fig. 3). The DCHM data were then triangulated by the Delaunay triangulation method [2, 3] to produce a three-dimensional polygon image. This was processed by a Laplacian smoothing filter [15, 37].

The point cloud image generated from the on-ground LIDAR data was registered and overlapped on the polygon image generated from airborne scanning LIDAR data by taking corresponding points between the two LIDAR images as the reference points (e.g., treetops or intersections of the trees). The blind regions within the polygon image of the airborne scanning LIDAR were identified by comparing the two images. The point cloud data equivalent to the blind regions, which were the canopies hidden by the *Liriodendron* and the understructure as shown in Fig. 6a and b, were extracted from the point cloud image to complement the blind regions. After the resolution of the extracted point cloud data was adjusted to that of the airborne LIDAR data, the point cloud data were three-dimensionally triangulated by Delaunay triangulation and the ball-pivoting algorithm [4] to produce three-dimensional polygon images. Finally, the polygon images from the airborne and on-ground LIDARs were merged.

2.7 Computation of the Biophysical Variables of Trees from the Final Three-Dimensional Model

The final three-dimensional model of *M. glyptostroboides* trees still included the ground surface. The height of the ground surface was identified from the height histogram of all point cloud data within the model. The histogram of point cloud data corresponding to the ground surface formed a large sharp peak including the lowest height. The trees and ground surface were separated on the peak.

Then, we computed the individual tree height, trunk diameter, and maximum canopy diameter and compared them with ground-truth data to evaluate the accuracy of the model. Tree trunks were defined as the portion from ground level to 1.3-m height, corresponding to the height of the lowest foliage, and the maximum canopy diameter was defined as the maximum external diameter on a horizontal cross-section at a certain height. We also computed more descriptive tree variables: canopy volume, trunk volume, and cross-sectional area.

3 Results

Figure 4a shows a three-dimensional view of the FP-mode DEM image of the study site where trees, buildings, streets, and railways are reproduced. The close-up image in Fig. 4b shows a detailed view of the French Formal Garden (white broken line in Fig. 1) where distinctive features such as rectangular flowerbeds, shrubberies surrounding the beds, and rows of trees arranged on either side can be seen. Although the canopy of each tree is reproduced properly, the image contains no information about the understructure of each tree, as shown by the cup-shaped image of each tree and shrub, because the measurement was made from the air. Figure 4c shows a three-dimensional view of the DTM image of the study site. This image yields ground-surface information, although the ground was covered with many trees. Ponds appear flat. Figure 4d shows the DCHM image constructed by subtracting the DTM image from the FP-mode DEM image. The DCHM gives the net canopy height of each tree without the influence of ground slope. The RMSE (root-mean-square error) of the heights of 166 trees extracted

from the DCHM was 0.30 m. The standard deviation was 0.26 m, and the mean error was -0.14 m. This result indicates that the tree heights were slightly underestimated.

Figure 5a and b shows three-dimensional point cloud images of an *L. tulipifera* and a *P. × yedoensis* produced by merging on-ground LIDAR data. The images show detailed features, including ramifications of branches, shapes of trunks, and distribution of leaves, without limitation of viewing angle.

Figure 6a shows three-dimensional views of the DCHM images of the three *M. glyptostroboides* trees (Fig. 3) after triangulation and smoothing (Fig. 2c). Regions A and B in Fig. 6a represent the blind regions in the airborne scanning LIDAR data. Region A is canopy covered by the huge *L. tulipifera* tree (see Fig. 3), and region B is understructure. Figure 6b shows a three-dimensional point cloud image obtained by merging on-ground LIDAR data measured from five measurement ground positions (see Figs. 2b and 3). Regions A and B in Fig. 6b correspond to those in Fig. 6a. The two regions within the three-dimensional point cloud image were extracted and triangulated. Then, they were merged with the helicopter-borne three-dimensional polygon image as shown in Fig. 6c and d (see Fig. 2c). An entire three-dimensional model of the three trees was thus produced by complementing the blind regions.

Table 1 shows biophysical variables of the three *M. glyptostroboides* trees obtained from the on-ground LIDAR image after merging, the final three-dimensional model obtained by combining data from both LIDARs, and ground-truth data. Tree height errors ranged from -0.13 to 0.31 m for the on-ground LIDAR image and from -0.05 to -0.73 m for the final model. The error of the trunk diameter was within 1 cm for both the on-ground LIDAR image and

Fig. 4 Three-dimensional views of FP-mode DEM, DTM, and DCHM images of the study site. **a** FP-mode DEM image. **b** Close-up of FP-mode DEM image of the French Formal Garden. **c** DTM image. **d** DCHM image

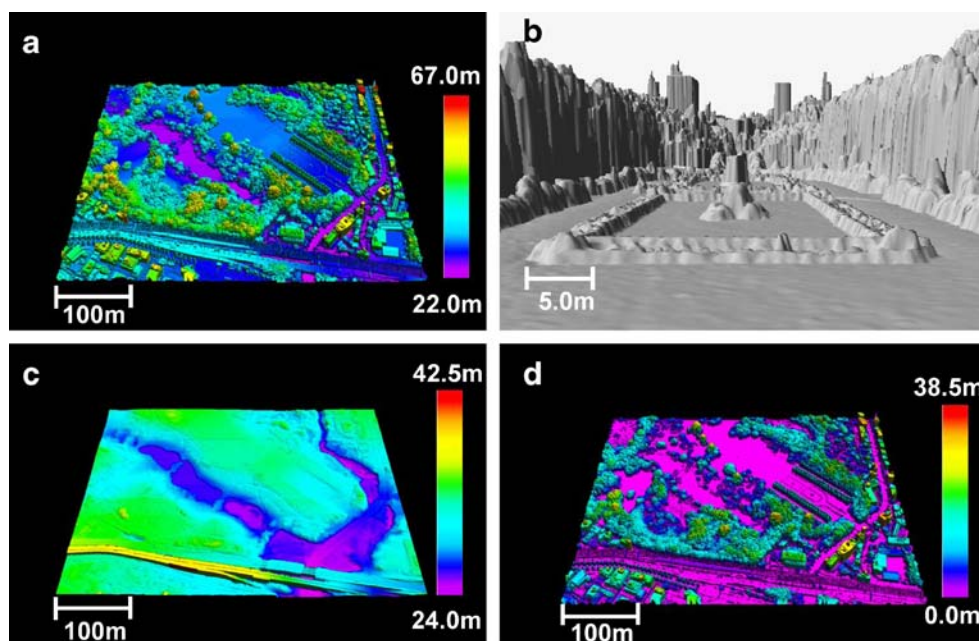
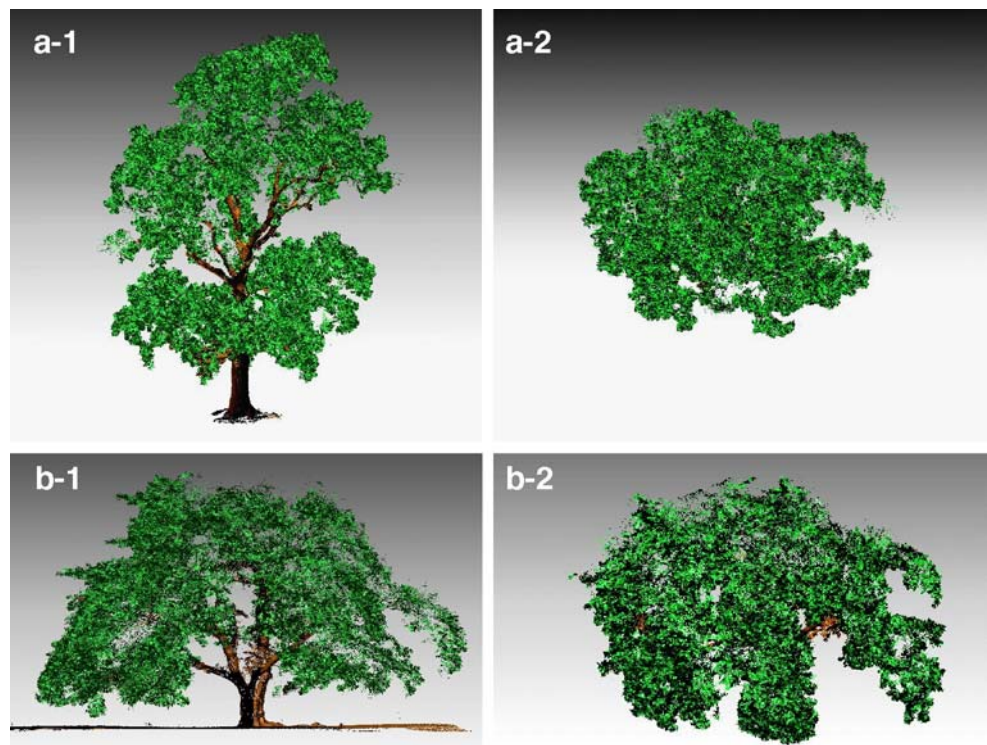


Fig. 5 Three-dimensional point cloud images (*side view and top view*) of isolated trees in the study area obtained by merging portable on-ground scanning LIDAR data. **a** *Liriodendron tulipifera*. **b** *Prunus* × *yedoensis*. Regions corresponding to leaves are colored *green* and others are colored *brown*



three-dimensional model. The final three-dimensional model was sliced at different heights and scales as shown in Fig. 7 to compute the trunk diameter, maximum canopy diameter, and canopy cross-sectional area. The error of the maximum canopy diameter ranged from -0.58 to 0.28 m.

The canopy volume, trunk volume, and canopy cross-sectional areas at 1.5 and 10 m heights of each tree ranged from 289.0 to 616.8 m³, 0.29 to 0.61 m³, 37.42 to 54.73 m², and 17.42 to 24.33 m², respectively. The total volume of the three trees was 1,464.5 m³.

Fig. 6 Combining airborne and portable on-ground scanning LIDAR images. **a** Airborne LIDAR images produced from the portion of DCHM data including three *Metasequoia glyptostroboides* trees. Regions *A* and *B* are blind regions. **b** Combined three-dimensional point cloud image of the *M. glyptostroboides* trees measured by on-ground LIDAR from five ground measurement positions. Regions *A* and *B* correspond to the blind regions in the airborne scanning LIDAR data. **c** and **d** Final three-dimensional model of the *M. glyptostroboides* trees (*side and top view*, respectively)

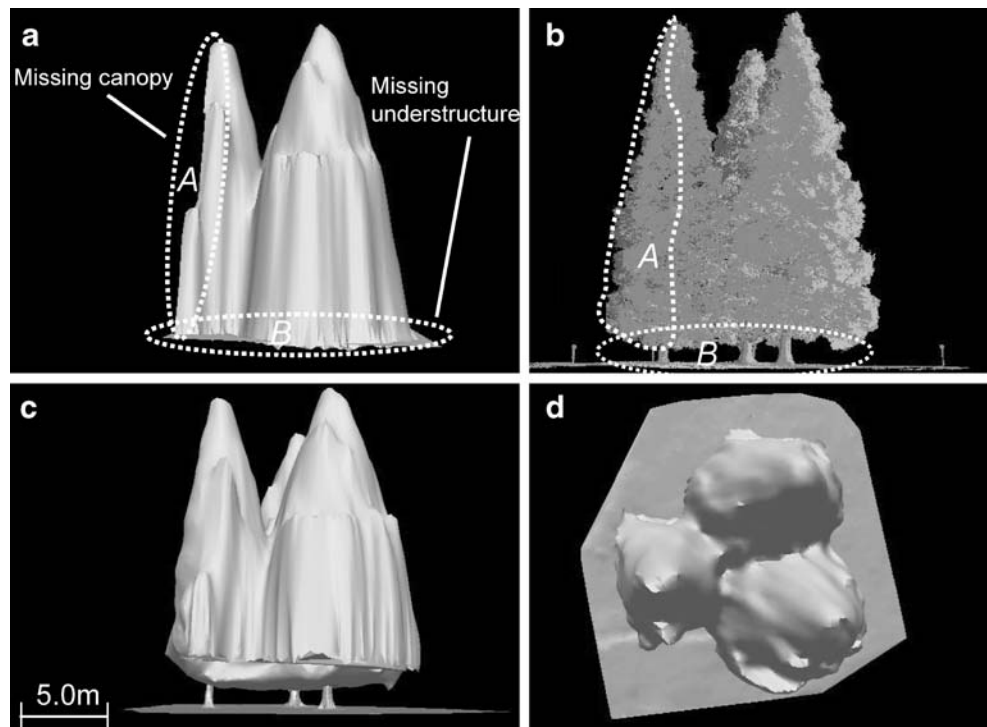


Table 1 Biophysical variables of three *Metasequoia glyptostroboides* trees obtained from the portable on-ground scanning LIDAR image, the final three-dimensional model, and ground-truth measurements

Tree	Height (m)	Maximum canopy diameter (m)		Canopy cross-section area (m ²)		Trunk diameter (cm)		Canopy volume (m ³)	Trunk volume (m ³)	Total volume ^b (m ³)
		h ₁ ^a	h ₂ ^a	h ₁ ^a	h ₂ ^a	h ₃ ^a	h ₄ ^a			
On-ground scanning LIDAR image	1	19.87	-	-	-	51.1	45.0	-	-	-
	2	20.37	-	-	-	65.8	55.6	-	-	-
	3	19.73	-	-	-	67.6	57.4	-	-	-
Model	1	19.27	7.86	5.29	17.42	51.1	45.0	289.0	0.29	289.3
	2	20.01	9.50	6.63	24.33	65.8	55.6	616.8	0.57	617.4
	3	19.25	9.40	6.02	22.54	67.6	57.4	557.2	0.61	557.8
Ground measurements	1	20.00	7.82	5.01	-	50.9	45.2	-	-	-
	2	20.06	9.79	7.15	-	65.7	55.6	-	-	-
	3	19.88	9.98	6.07	-	67.4	57.5	-	-	-

Heights h₁ to h₄ correspond to those in Fig. 7.

^a h₁–h₄: height from the ground

^b Total volume: canopy volume + trunk volume

4 Discussion

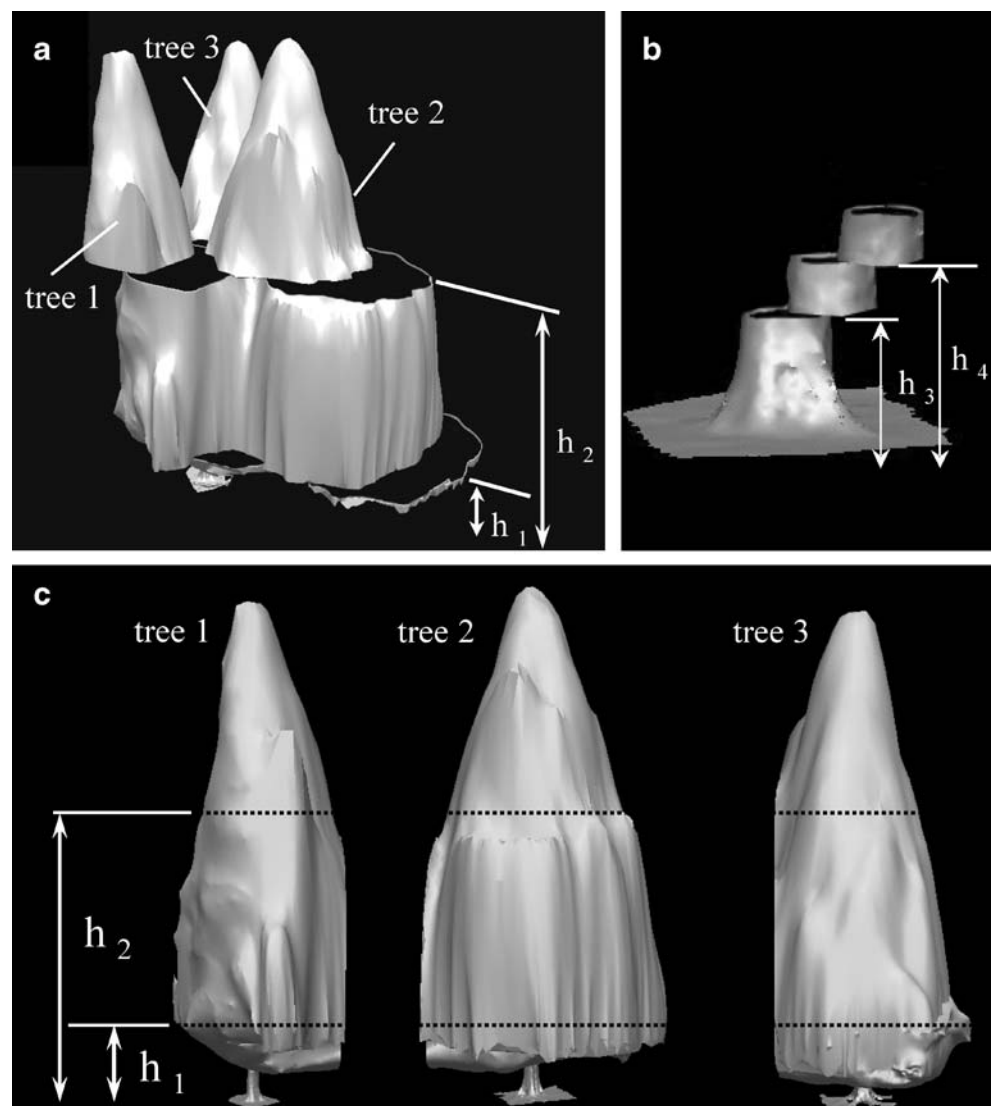
Airborne scanning LIDAR allowed the generation of precise visual models of the study area as shown in Fig. 4. These visual models provided not only precise surface information of trees and constructions in the park but also information about undulations of the ground in spite of the presence of many trees. The result shows the capability of airborne LIDAR for three-dimensional visualization of an urban park. The heights of 166 coniferous and broadleaf trees within the study area could be estimated with only slight underestimation (RMSE=0.30 m), so the data would be suitable for managing and studying the park. The underestimation would have been caused by misdetection of treetops. As a treetop is a very small target, LIDAR will often miss it, resulting in underestimation of tree heights [20, 25, 30].

Although the airborne scanning LIDAR provided a precise three-dimensional visual model of the study area, there existed blind regions, as shown in Fig. 4b, by the cup-shaped images of trees and shrubs. These blind regions reduce the visual quality of the LIDAR-derived image. In addition, tree variables for the lower parts of trees, such as trunk diameter and basal area, are not available. This shows the limitation of airborne LIDAR in the three-dimensional visualization of an urban park and quantification of tree variables.

The on-ground LIDAR could capture the lower parts of individual trees, as shown in Fig. 5, owing to the measurements from several ground positions surrounding the trees. Such precise three-dimensional images without blind regions would be as appropriate for the visual assessment of urban parks as recent realistic three-dimensional models of individual trees based on several algorithms such as texture mapping, AMAP, and the TREE system [14, 23]. In addition, the LIDAR-derived images are more advantageous than those three-dimensional models in a point that variables of real trees can be obtained from the images, as shown here. On the other hand, some regions of dense trees may not be captured by on-ground LIDAR. In this study, parts of the canopies of three *M. glyptostroboides* were missed owing to overlapping of trees. The blind region could affect the visual quality of the LIDAR-derived image and limit the estimation of tree variables.

Combination of the airborne and on-ground LIDAR data provided a complete image of trees without blind regions, allowing visual assessment without limitation of viewpoints. In addition, several tree variables that could not have been estimated from airborne or on-ground LIDAR data alone were estimated from the complete tree model by the use of image processing techniques, as shown in Fig. 7. Any region of the model can be selected and sliced freely. The estimated variables also include some that are difficult

Fig. 7 Final three-dimensional models of the *Metasequoia glyptostroboides* sliced at different heights and separated individually. **a** Sliced canopy. **b** Sliced trunk. **c** Separated individual trees. Heights h_1 to h_4 are slice positions



to measure even with actual ground measurements, i.e., canopy volume, trunk volume, and canopy cross-sectional area. These variables obtained through the image processing may provide additional knowledge for understanding the botanical and environmental functions of urban parks.

5 Conclusions

The present study demonstrates three-dimensional modeling of an urban park and trees using airborne and portable on-ground scanning LIDARs. First, we confirmed the capability of these LIDARs for three-dimensional visualization of an urban park and quantification of tree variables. The DCHM and DTM generated from airborne LIDAR data provided precise images of the canopy and ground surfaces. Tree heights were only slightly underestimated from the DCHM images. On-ground LIDAR provided

images of individual trees with detailed features. Tree variables such as trunk diameter and tree height were estimated accurately from the images. Blind regions within both LIDAR images limited the capability of either for three-dimensional visualization of the park and quantification of tree variables. Then, airborne and on-ground LIDAR were combined to complement the blind regions, and a complete three-dimensional model of three standing trees was created. The model allowed not only visual assessment from all viewpoints but also quantitative estimation of more descriptive tree variables. The study demonstrates our basic concept for composite remote sensing by airborne and on-ground scanning LIDARs. Only three trees were reproduced in this study; in the future, it will be desirable to image more trees in parks to enhance the quality of visual and quantitative assessment for planning and managing urban parks and contributing to a better understanding of their environmental functions.

References

1. Avissar, R. (1996). Potential effects of vegetation on the urban thermal environment. *Atmospheric Environment*, *30*, 437–448.
2. Bajaj, C. L., Bernardini, F., & Xu, G. (1995). Automatic reconstruction of surfaces and scalar fields from 3D scans. *Proceedings of SIGGRAPH '95 International Conference on Computer Graphics and Interactive Techniques* (pp. 109–118). New York: ACM SIGGRAPH.
3. Baker, T. J. (1989). Developments and trends in three-dimensional mesh generation. *Applied Numerical Mathematics*, *5*, 275–304.
4. Bernardini, F., Mittleman, J., Rushmeier, H., Silva, C., & Taubin, G. (1999). The ball-pivoting algorithm for surface reconstruction. *IEEE Transactions on Visualization and Computer Graphics*, *5*, 349–359.
5. Besl, P. J., & McKay, N. D. (1992). A method for registration of 3-D shapes. *IEEE Transactions on Pattern Analysis and Machine Intelligence*, *14*, 239–256.
6. Bishop, I. D., & Rohrmann, B. (2003). Subjective responses to simulated and real environments: A comparison. *Landscape and Urban Planning*, *65*, 261–277.
7. Caldas, C. H., Chi, S., Teizer, J., & Gong, J. (2006). Intelligent computing and sensing for active safety on construction sites. *Lecture Notes in Artificial Intelligence*, *4200*, 101–108.
8. Chiesura, A. (2004). The role of urban parks for the sustainable city. *Landscape and Urban Planning*, *68*, 129–138.
9. Forlani, G., Nardinocchi, C., Scaioni, M., & Zingaretti, P. (2006). Complete classification of raw LIDAR data and 3D reconstruction of buildings. *Pattern Analysis and Applications*, *8*, 357–374.
10. Gallo, K. P., McNab, A. L., Karl, T. R., Brown, J. F., Hood, J. J., & Tarpley, J. D. (1993). The use of a vegetation index for assessment of the urban heat-island effect. *International Journal of Remote Sensing*, *20*, 2223–2230.
11. Hosoi, F., & Omasa, K. (2006). Voxel-based 3D modeling of individual trees for estimating leaf area density using high-resolution portable scanning LIDAR. *IEEE Transactions on Geoscience and Remote Sensing*, *44*, 3610–3618.
12. Hosoi, F., Yoshimi, K., Shimizu, Y., & Omasa, K. (2005). 3-D measurement of trees using a portable scanning LIDAR. *Phyton*, *45*, 497–500.
13. Hyde, P., Nelson, R., Kimes, D., & Levine, E. (2007). Exploring LiDAR-RaDAR synergy – Predicting aboveground biomass in a southwestern ponderosa pine forest using LiDAR, SAR and InSAR. *Remote Sensing of Environment*, *106*, 28–38.
14. Jaeger, M., & de Reffye, P. (1992). Basic concepts of computer simulation of plant-growth. *Journal of Biosciences*, *17*, 275–291.
15. Ji, Z., Liu, L., & Wang, G. (2005). A global Laplacian smoothing approach with feature preservation. *Proceedings of the Ninth International Conference on Computer Aided Design and Computer Graphics* (pp. 269–274). Hong Kong, China: IEEE.
16. Kaplan, S., & Kaplan, R. (1989). *The experience of nature. A psychological perspective*. Cambridge: Cambridge University Press.
17. Lam, K. C., Ng, S. L., Hui, W. C., & Chan, P. K. (2005). Environmental quality of urban parks and open spaces in Hong Kong. *Environmental Monitoring and Assessment*, *111*, 55–73.
18. Lange, E. (2001). The limits of realism: perceptions of virtual landscapes. *Landscape and Urban Planning*, *54*, 163–182.
19. Lange, R., & Seitz, P. (2001). Solid-state time-of-flight range camera. *IEEE Journal of Quantum Electronics*, *37*, 390–397.
20. Lefsky, M. A., Cohen, W. B., Parker, G. G., & Harding, D. J. (2002). LIDAR remote sensing for ecosystem studies. *BioScience*, *52*, 19–30.
21. Lovell, J. L., Jupp, D. L. B., Culvenor, D. S., & Coops, N. C. (2003). Using airborne and ground-based ranging LIDAR to measure canopy structure in Australian forests. *Canadian Journal of Remote Sensing*, *29*, 607–622.
22. Maltamo, M., Eerikäinen, K., Pitkänen, J., Hyypä, J., & Vehmas, M. (2004). Estimation of timber volume and stem density based on scanning laser altimetry and expected tree size distribution functions. *Remote Sensing of Environment*, *90*, 319–330.
23. Muhar, A. (2001). Three-dimensional modeling and visualization of vegetation for landscape simulation. *Landscape and Urban Planning*, *54*, 5–17.
24. Murakami, H., Nakagawa, K., Hasegawa, H., Shibata, T., & Iwanami, E. (1999). Change detection of buildings using an airborne laser scanner. *ISPRS Journal of Photogrammetry and Remote Sensing*, *54*, 148–152.
25. Næsset, E., Gobakken, T., Holmgren, J., Hyypä, H., Hyypä, J., Maltamo, M., et al. (2004). Laser scanning of forest resources: The Nordic experience. *Scandinavian Journal of Forest Research*, *19*, 482–499.
26. Oggier, T., Lustenberger, F., & Blanc, N. (2006). Miniature 3D TOF camera for real-time imaging. *Lecture Notes in Artificial Intelligence*, *4021*, 212–216.
27. Omasa, K. (2002). Diagnosis of stomatal response and gas exchange of trees by thermal remote sensing. In K. Omasa, H. Saji, S. Youssefian, & N. Kondo (Eds.), *Air pollution and plant biotechnology – prospects for phytomonitoring and phytoremediation* (pp. 343–359). Tokyo: Springer.
28. Omasa, K., Akiyama, Y., Ishigami, Y., & Yoshimi, K. (2000). 3-D remote sensing of woody canopy heights using a scanning helicopter-borne LIDAR system with high spatial resolution. *Journal of Remote Sensing Society of Japan*, *20*, 394–406.
29. Omasa, K., Hosoi, F., & Konishi, A. (2007). 3D LIDAR imaging for detecting and understanding plant responses and canopy structure. *Journal of Experimental Botany*, *58*, 881–898.
30. Omasa, K., Qiu, G. Y., Watanuki, K., Yoshimi, K., & Akiyama, Y. (2003). Accurate estimation of forest carbon stocks by 3-D remote sensing of individual trees. *Environmental Science & Technology*, *37*, 1198–1201.
31. Omasa, K., Tobe, K., & Kondo, T. (2002). Absorption of organic and inorganic air pollutants by plants. In K. Omasa, H. Saji, S. Youssefian, & N. Kondo (Eds.), *Air pollution and plant biotechnology – prospects for phytomonitoring and phytoremediation* (pp. 155–178). Tokyo: Springer.
32. Omasa, K., Urano, Y., Oguma, H., & Fujinuma, Y. (2002). Mapping of tree position of *Larix leptolepis* woods and estimation of diameter at breast height (DBH) and biomass of the trees using range data measured by a portable scanning LIDAR. *Journal of Remote Sensing Society of Japan*, *22*, 550–557.
33. Sequeira, V., Gonçalves, J. G. M., & Ribeiro, M. I. (1995). 3D environment modeling using laser range sensing. *Robotics and Autonomous Systems*, *16*, 81–91.
34. Shah, S., & Aggarwal, J. K. (1997). Mobile robot navigation and scene modeling using stereo fish-eye lens system. *Machine Vision and Applications*, *10*, 159–173.
35. Surmann, H., Nüchter, A., & Hertzberg, J. (2003). An autonomous mobile robot with a 3D laser range finder for 3D exploration and digitalization of indoor environments. *Robotics and Autonomous Systems*, *45*, 181–198.
36. Tanaka, T., Park, H., & Hattori, S. (2004). Measurement of forest canopy structure by a laser plane range-finding method improvement of radiative resolution and examples of its application. *Agricultural and Forest Meteorology*, *125*, 129–142.
37. Taubin, G. (1995). A signal processing approach to fair surface design. *Proceedings of SIGGRAPH '95 International Conference on Computer Graphics and Interactive Techniques* (pp. 351–358). New York: ACM SIGGRAPH.
38. Ulrich, R. S. (1981). Natural versus urban scenes: Some psychophysiological effects. *Environment and Behavior*, *13*, 523–556.